DOI 10.1007/s11595-013-0672-y

Water Distribution and Removal along the Flow Channel in Proton Exchange Membrane Fuel Cells

DING Gangqiang[1,4], TANG Heqing[1], LUO Zhiping[2], TU Zhengkai[2*], PEI Houchang[3], LIU Zhichun[3], LIU Wei[3]

(1.College of Chemistry and Chemical Engineering, Huazhong University of Science and Technology, Wuhan 430074, China; 2.State Key Laboratory of Advanced Technology for Materials Synthesis and Processing, Wuhan University of Technology, Wuhan 430070, China;3. College of Energy and Power Engineering, Huazhong University of Science and Technology, Wuhan 430074, China;4 Power Battery Division, Wuhan Institute of Marine Electric Propulsion, Wuhan 430064, China)

Abstract: Distribution expressions of total gas pressure and partial water vapor pressure along the channel direction were established based on lumped model by analyzing pressure loss in the channel and gas diffusion in the layer. The mechanism of droplet formation in the flow channel was also analyzed. Effects of the relative humidity, working temperature and stoichiometry on liquid water formation were discussed in detail. Moreover, the force equilibrium equation of the droplet in the flow channel was deduced, and the critical flow velocity for the water droplet removal was also addressed. The experimental results show that the threshold position of the liquid droplet is far from the inlet with the increase of temperature, and it decreases with the increase of the inlet total pressure. The critical flow velocity decreases with the increase of the radius and the working pressure.

Key words: proton exchange membrane fuel cells; pressure loss; water distribution; water removal

1 Introduction

Proton exchange membrane fuel cell (PEMFC) is widely developed in the world because of its low noise, low/zero emission, long lifetime, great reliability, and high energy conversion efficiency[1-6]. As one of the key components in PEMFC, gas diffusion layer is the porous connecting channel from which the fuel gases flow into the catalyst layer. While the fuel cell is under operation, fuel gases are usually humidified and liquid water is also generated at cathode. Thus, it is necessary to discharge the generated water from the gas diffusion layer (GDL) to avoid flooding electrode during the fuel cell operation, which can greatly reduce the performance of cell[7-9].

As water management in PEMFC is one of the critical factors affecting the cell performance, it is quite important to understand the transfer behavior and distribution of water in the gas diffusion layer. Zhan *et al*[10] studied how the thickness of GDL affected the water distribution in the diffusion layer using numerical simulation. It was concluded that under steady-state condition, the liquid water flowrate through the GDL increased as contact angle, and porosity increased as the GDL thickness decreased. When a micro-porous layer (MPL) is placed between the catalyst layer and the GDL, the liquid saturation is redistributed across the MPL and GDL, which improves the liquid water draining performance. Tuber[11] and Yang *et al*[12] experimentally observed the permeation of water from the diffusion layer to flow field channel, water droplet formation and growth, and then water block in the channel. They measured the relationship between cell performance and water block in the channel, and investigated the effects of different air flowrate, temperature, humidity, and hydrophobicity of diffusion layer on the cell performance. Using a transparent cathode, they found that the properties of applied carbon papers directly influenced the accumulation of produced water in the gas channels. The produced water can even totally clog the flow channels, resulting in enormous performance losses. Generally, if the partial pressure exceeds the saturated pressure, water vapor in the flow channel and

©Wuhan University of Technology and SpringerVerlag Berlin Heidelberg 2013

(Received: Feb. 19, 2012; Accepted: Apr. 8, 2012)

DING Gangqiang(丁刚强):Ph D;E-mail:ty2010@126.com

*Corresponding author: TU Zhengkai (涂正凯): Assoc. Prof. ; Postdoctoral; E-mail: tzklq@whut.edu.cn

Funded by the National Natural Science Foundation of China (Nos. 51036003, 50906026, 20876121, and 51276071), and the Fundamental Research Funds for the Central Universities (2012IV084 and 2011TS079)

GDL may transform into liquid drop. The formation of the liquid water droplet requires condensing nucleus and sub-cool. The fibrous fabric of the GDL provides numbers of nuclei for the water condensation. Due to the exothermic reaction near the catalyst layer and the good heat exchange capability of the land, temperature difference can be generated between the flow gas and the surface of the land. Moreover, Meng and Wang[13] pointed out that due to the assembling and transporting effect of the land on the current, the current transportation in the land was higher than that in the channel. Hence, the nuclei near the land present higher electrical adsorption capability of the water molecule in the GDL. Cao[14] pointed out that larger contact angle was helpful for the droplet condensation, and the optimal contact angle was 111-114°. As a consequence, droplets are usually formed in the interface between the land and channel[11,15,16]. Therefore, when water vapor is over-saturated, liquid can be easily condensed from humid gas and transmit to the surface of diffusion layer by capillary force[17,18].

In this study, the expression of water distribution along the flow channel in the cathode was established through analysis of liquid water formation in the gas diffusion layer, and based on the force equilibrium equation of a droplet, the critical flow velocity for the droplet removal was obtained. The results presented here could be theoretical guidance on the design of flow field for PEMFC.

2 Theoretical framework

2.1 Water distribution

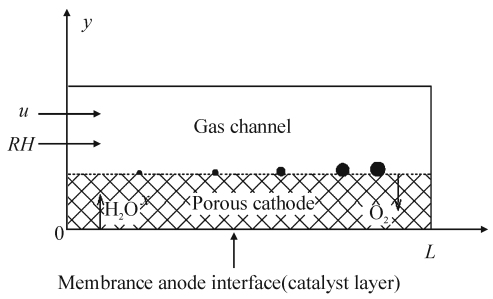

Fig.1 Schematic of gas flow along the flow channel

To simplify the deduction, the following assumptions are made: gas is considered to be ideal gas; all supersaturated water in fuel gases is condensed into liquid state in the flow channel; and the amount of reacting gas at unit area in the flow direction is uniform.

Fig.1 shows the schematic of gas flow in the channel and gas diffusion layer. According to the thermodynamics equation, the relationship between saturated water vapor pressure P_{sat} and temperature T can be expressed as follows[19]:

$$\lg p_{sat} = -2.1794 + 2.953\times10^{-2}(T-273.15) - 9.1837\times 10^{-5}(T-273.15)^2 + 1.4454\times10^{-7}(T-273.15)^3 \quad (1)$$

In Fig.1, the inlet gas pressure defines as p_0, cell working temperature as T, relative humidity as RH, channel length as L, width as a, height as b, and stable working current density as i (A•cm^{-2}). According to the ideal gas equation, in x direction, the gas velocity is considered as constant. Within time change dt, for the displacement dx, the pressure drop along the direction of movement due to the consume of gas can be expressed as :

$$\mathrm{d}p \cdot abu\mathrm{d}t = \dot{n}_{total} aRT\mathrm{d}x\mathrm{d}t \quad (2)$$

where, u is gas velocity, and $\dot{n}_{total}$ is the total molar consume rate per area. By integrating the expression (2), one can obtain the pressure loss as follows:

$$p = \frac{nRT}{abu} \quad (3)$$

$$\Delta p_x = \frac{\dot{n}_{total} RTx}{bu} \quad (4)$$

where, n is the molar flow rate. Defined the gas flow and water vapor flow rate at inlet as n_0 and n_{H_2O}, pressure at x in the cathode can be expressed as:

$$p_x = p_0 - \Delta p_{channel} - \Delta p_{gdl} - \frac{1}{2}\dot{n}\frac{RTx}{bu} + (2\alpha+1)\dot{n}\frac{RTx}{bu} \quad (5)$$

where, α is the net water transport coefficient, and the second item in the right is the pressure loss due to the gas movement in channel, the third item is the pressure loss due to the gas diffusion in the diffusion layer, the fourth item is the pressure loss due to the consume of oxygen, the fifth item is pressure increment due to the consume of water molecular dragged by ion from the anode and the sixth item is pressure increment due to the formed water vapor. Here, $\dot{n} = i/2F$ (calculating according to the per area consume of hydrogen), F is the Faraday constant. The vapor partial pressure at x in the cathode can be expressed as:

$$p_{H_2O,x} = p_x \frac{n_{H_2O} + 2\alpha\dot{n}\cdot a\cdot x + \dot{n}\cdot a\cdot x}{n_0 + \dot{n}\cdot a\cdot x + 2\alpha\dot{n}\cdot a\cdot x - \frac{1}{2}\dot{n}\cdot a\cdot x}$$

$$= [p_0 - \Delta p_{channel} - \Delta p_{gdl} + \frac{(2\alpha + \frac{1}{2})\dot{n}RTx}{bu}]$$

$$\frac{\frac{RH\cdot p_{sat}abu}{RT} + (2\alpha+1)\dot{n}\cdot a\cdot x}{\frac{p_0 abu}{RT} + \dot{n}(2\alpha + \frac{1}{2})\cdot a\cdot x} \tag{6}$$

According to the magnitude analysis, $\Delta p_{channel} + \Delta p_{gdl} << p_0$. Hence,

$$p_{H_2O,x} = (p_0 - \frac{\dot{n}(2\alpha + \frac{1}{2})RTx}{bu})\cdot$$

$$\frac{\frac{RH\cdot p_{sat}\cdot a\cdot b\cdot u}{RT} + (2\alpha+1)\dot{n}\cdot a\cdot x}{\frac{p_0\cdot a\cdot b\cdot u}{RT} + \dot{n}(2\alpha + \frac{1}{2})\cdot a\cdot x}$$

$$= [p_0 - \frac{\dot{n}(2\alpha + \frac{1}{2})RTx}{bu}]\cdot$$

$$\frac{RH\cdot p_{sat} + \frac{(2\alpha+1)\dot{n}RTx}{bu}}{p_0 - \frac{\dot{n}(2\alpha + \frac{1}{2})RTx}{bu}}$$

$$= RH\cdot p_{sat} + \frac{(2\alpha+1)\dot{n}RTx}{bu} \tag{7}$$

$$= RH\cdot p_{sat} + \frac{p_0}{n_0}\cdot(2\alpha+1)\dot{n}\cdot a\cdot x$$

If the fuel gas in the cathode is oxygen, Eq.(7) can be written as

$$p_{H_2O,x} = RH\cdot p_{sat} + \frac{p_0 - RH\cdot p_{sat}}{0.5\lambda\dot{n}\cdot a\cdot L}\cdot(2\alpha+1)\dot{n}\cdot a\cdot x$$

$$= RH\cdot p_{sat} + (p_0 - RH\cdot p_{sat})\frac{(2\alpha+1)}{0.5\lambda}\cdot\frac{x}{L} \tag{8}$$

If the fuel gas in the cathode is air, Eq.(7) can be written as

$$p_{H_2O,x} = RH\cdot p_{sat} + \frac{p_0 - RH\cdot p_{sat}}{2.38\lambda\dot{n}\cdot a\cdot L}\cdot(2\alpha+1)\dot{n}\cdot a\cdot x$$

$$= RH\cdot p_{sat} + (p_0 - RH\cdot p_{sat})\frac{(2\alpha+1)}{2.38\lambda}\cdot\frac{x}{L} \tag{9}$$

where, λ is the stoichiometry of reacting gas. When water vapor get saturated, one can obtain,

$$p_{H_2O,x} = RH\cdot p_{sat} + (p_0 - RH\cdot p_{sat})\cdot \frac{(2\alpha+1)}{2.38\lambda}\cdot\frac{x}{L} \approx p_{sat} \tag{10}$$

Therefore, the threshold position of the liquid can be obtained,

$$\frac{x}{L} = \frac{p_{sat}(1-RH)}{(p_0 - RH\cdot p_{sat})}\cdot\frac{2.38\lambda}{(1+2\alpha)} \tag{11}$$

2.2 Liquid removal

According to the Ref.[11], droplet will gradually gather into swollen droplet, and eventually clog the flow channel. Therefore, it is necessary to remove the droplet before gathering.

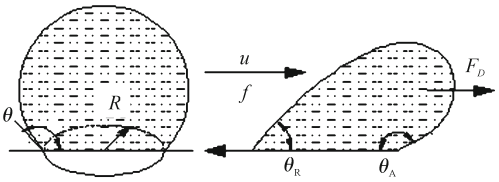

Fig.2 Force balance of the liquid droplet

Furmidge[20] and David[21] pointed out that the threshold resistance which the droplet movement needs to overcome could be calculated (Fig.2):

$$f = \pi\sigma R_c(\cos\theta_R - \cos\theta_A) \tag{12}$$

where, R_c is the radius of the bottom, σ is the liquid-gas surface tension, θ_A and θ_R are the advancing and receding angles the of droplet, respectively. Tu *et al*[22] analyzed the mechanical equilibrium of the drop on the rough surface related to the contact angle hysteresis and deduced that in the critical state, the relations of θ_A, θ_R and the Young's contact angel θ can be expressed as

$$\cos\theta = \frac{\cos\theta_A + \cos\theta_R}{2} \tag{13}$$

The research results in the Ref.[23] indicated that the impact of wind force F_D on the droplet was:

$$F_D = C_D A_p \frac{\rho_a u^2}{2} \tag{14}$$

where, u is gas velocity, C_D is resistance coefficient and the value is 1.22, and ρ_a is the density of the mixture gas. The effective area of flow wind can be calculated by $A_P = R_c^2 \frac{\theta_M - \sin\theta_M \cdot \cos\theta_M}{\sin^2\theta_M}, \theta_M = \frac{\theta_A + \theta_R}{2}$. The volume of the droplet coronal can be expressed as,

$$V = \frac{1}{3}\pi R_c^3 \frac{(1-\cos\theta)^2(2+\cos\theta)}{\sin^3\theta} \tag{15}$$

Consequently, droplet removal requires,

$$C_D A_p \frac{\rho_a u^2}{2} + \frac{1}{3}\pi\rho g R_c^3 \frac{(1-\cos\theta)^2(2+\cos\theta)}{\sin^3\theta} \cdot \sin\alpha \geqslant \pi\sigma R_c(\cos\theta_R - \cos\theta_A) \tag{16}$$

where, the first and the second items in the left are the wind force and gravity, respectively, and the item on the right is the hysteresis force.

In the Ref.[14], the critical curvature radius r_c and critical volume v_c of a droplet coronal for critical condensing/departure can be expressed as,

$$r_c = \frac{2\sigma v_{mol}}{RT\ln(p_\beta / p_{sat})}\left[\frac{2+\cos\theta_c(1+\cos\theta_c)}{(1-\cos\theta_c)(2+\cos\theta_c)}\right]$$

$$v_c = \frac{2}{3}\pi r_c^3 - \pi\pi r_c^3\cos\theta_c + \frac{1}{3}\pi r_c^3\cos\theta_c^3 = \frac{1}{3}\pi\left[\frac{2\sigma v_{mol}}{RT\ln(p_\beta / p_{sat})}\right]^3\left[\frac{2+\cos\theta_c(1+\cos\theta_c)}{(1-\cos\theta_c)(2+\cos\theta_c)}\right]^3 \cdot (2-3\cos\theta+\cos^3\theta)$$

where, v_{mol} is the molar volume, p_β is the liquid-vapor equilibrium pressure and θ_c is the critical contact angle.

$$\frac{dv_c}{d\theta_c} = \frac{d}{d\theta_c}\left\{\left[\frac{2+\cos\theta_c(1+\cos\theta_c)}{(1-\cos\theta_c)(2+\cos\theta_c)}\right]^3 \cdot (2-3\cos\theta+\cos^3\theta)\right\} = 0 \tag{17}$$

The minimum critical volume can be got when $\theta_c \approx 111^\circ$ and due to the minimum energy analysis, the minimum critical chemistry potential μ_c can also be reach at $\theta_c \approx 111^\circ$ in this literature, hence, the critical departure angle in this paper is considered as 111°.

3 Results and discussion

3.1 Distribution of water vapor partial pressure

According to Eq.(9), water vapor pressure increases with the distance, and to investigate the effects of the *RH*, working pressure and stoichiometry on the water distribution and condensing process, the net water transport coefficient was taken as zero for convenience in Figs.3-7. Fig.3 shows the evaluation of the saturated pressure and relative humidity (*RH*) corresponding to the temperature form 333(60 ℃) to 353 K(80 ℃). As can be seen, temperature has more notable effect on the RH than the saturated pressure does. When the temperature decreases by 2 K, the *RH* decreases by 8%. While the temperature further decreases to 343 K, the RH drops to 65.8%. As a consequence, if there is a temperature difference between the wall of flow channel and the gas, large amount of liquid water will be condensed from the fuel gas.

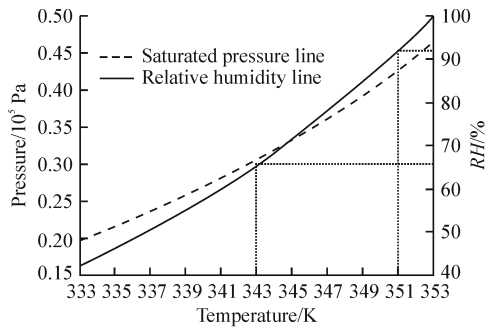

Fig.3 Evaluation of the saturated pressure and *RH* corresponding to the temperature form 60 to 80 ℃

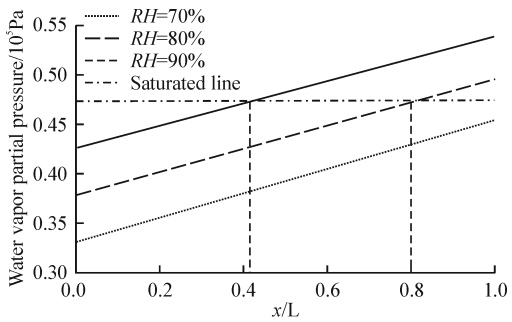

Fig.4 Differences of water vapor partial pressure under different *RH*s (λ=4, α=0)

Fig.4 shows the differences of water vapor partial pressure under different *RH*. Without condensing, the partial pressure of water vapor increases along the gas flow direction at different *RH*, and reaches the maximum at the outlet. The threshold position of the saturated pressure is closer to the inlet with the increase of *RH*. When *RH* is 70%, it even can not reach the saturated point at the outlet, whereas at *RH* of 90%, it is merely the 42% distance of the channel.

3.2 The location of liquid-vapor interface

Fig.5 shows the position of liquid-vapor interface at different temperatures. As can be seen, the threshold position of the liquid droplet is farther from the inlet

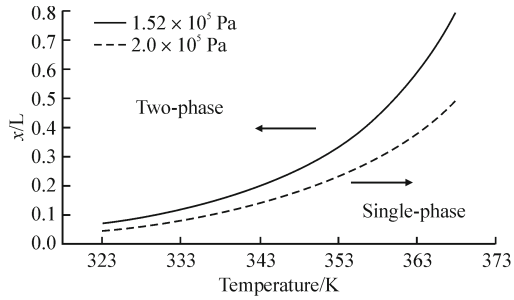

Fig.5 Location of liquid-vapor interface under different temperatures (λ=4, RH=80%)

with the increase of temperature. The reason is that saturated vapor pressure of the water increases rapidly with the temperature, and larger reactive area is needed to absorb more water molecules. Moreover, the distance of the threshold position decreases with increasing of the inlet total pressure. The reason is that the absolute water vapor pressure along the flow channel increases with increasing of the working pressure due to the generation of water vapor.

3.3 Liquid generation

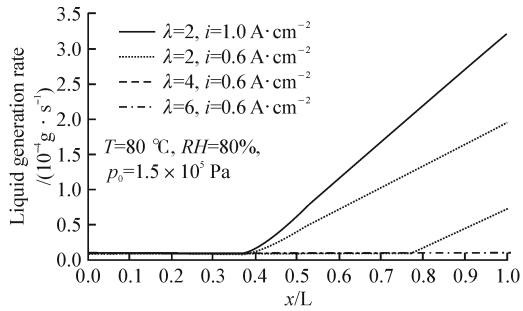

Fig.6 Effects of the stoichiometry and current density on liquid generation rate

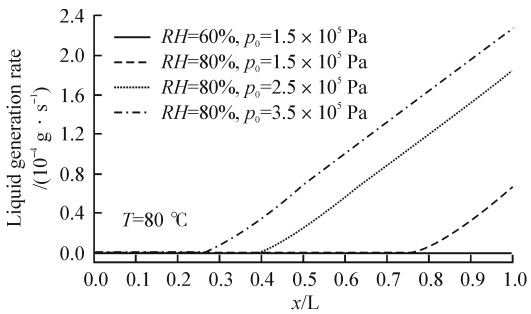

Fig.7 Effect of working pressure on liquid generation rate

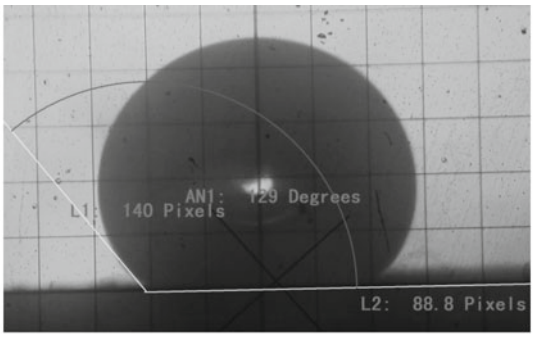

Fig.8 The apparent contact angel of a hydrophobic GDL

Fig.6 shows the effects of the stoichiometry and the current density on the liquid water generation rate. As can be seen, until the water vapor gets saturated, there is no liquid water generating in the channel. Besides, the position where the liquid water starts to generate is further from the inlet as the stoichiometry increased. However, the liquid water generates more quickly when the distance is longer. When the stoichiometry is 2, the rate at the same position increases as the current density increases from 0.6 A•cm^{-2} to 1.0 A•cm^{-2}. On the contrary, the rate for liquid water generation decreases as the stoichiometry increases from 2 to 6 when the current density is constant at 0.6 A•cm^{-2}.

3.4 Critical flow velocity

In the Ref.[14], it was stated that the optimal contact angle for the water droplet condensation was 111-114°. Hence, the receding angle θ_R of the critical removal can be chosen as 111°. Fig.8 shows the apparent contact angle θ(129°) of a hydrophobic GDL. According to Eq.(13), θ_A is calculated as 154.2°, and the parameters used for calculation are shown in Table 1.

Table 1 Parameters used for calculation

Property	Liquid water /60 ℃	Water vapor /60 ℃	Liquid water /60 ℃	Water vapor /60 ℃	Air (1.52 × 10^5 Pa) /80 ℃
ρ/(kg · m^{-3})	983.1	0.130	0.294	971.8	1.637
σ/(N · m^{-1})	0.067 2	–	0.064 4	–	–

3.4.1 Effect of tilted angle

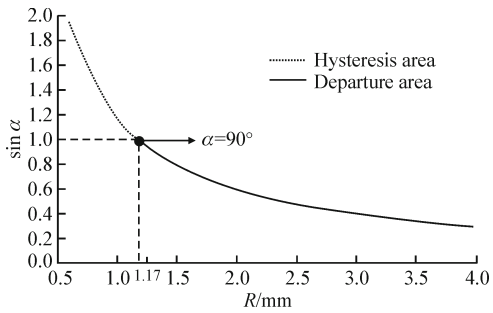

Fig.9 Effect of tilted angle on departure radius

Fig.9 shows the effect of the tilted angel on departure radius at temperature of 80°C. It can be seen that, without regard to the effect of the wind force, when radius is less than 1.17 mm (at this time, sinα is invalid, as the dotted line in Fig.9), the viscous force plays the leading role, which means the gravity of droplet itself cannot overcome the viscous force, the droplet will be stuck on the slope. While the radius is larger than 1.17mm, the gravity play the leading role,

the droplet will depart spontaneously from the slope, and the tilted angle for self-slipping down decrease quickly as the increase of radius.

3.4.2 Assisted drainage by gravity

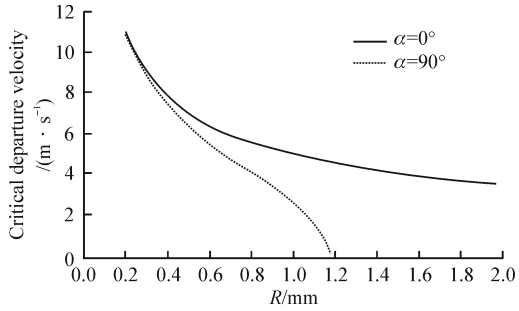

Fig.10 Critical velocity in horizontal and vertical position

Fig.10 shows the relationship between critical airflow velocity and radius at horizontal and vertical positions. It can be seen that, at small radius, the viscous force plays the leading role, gravity don't affect airflow very much. With the increase of radius, the critical velocity decrease more quickly in vertical position than that in horizontal position. The water removal ability can be enhanced by using gravity itself.

3.4.3 Effect of working pressure

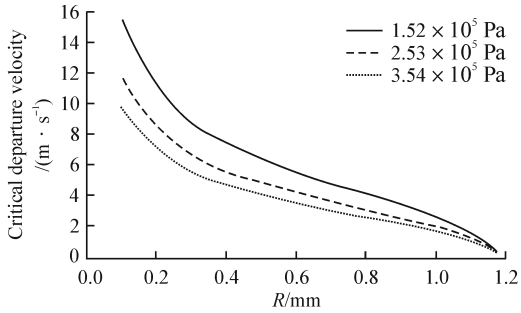

Fig.11 Pressure effect on critical velocity in vertical position

Fig.11 is the relationship between critical velocity and radius in vertical position. It can be seen that, critical velocity of droplet with same radius decreases with the increase of wording pressure. When the radius is small, pressure has an apparent effect on the airflow velocity, while for a droplet in the spontaneous departure area, this effect can be neglected, it could be that, with the increase of radius, the gravity will play a leading role, and the effect of wind force is weaken.

4 Conclusions

The threshold position of the liquid droplet is increasing with the increase of the temperature, and decreasing with the increase of the inlet total pressure. The critical flow velocity decreases with the increase of the radius and the working pressure. The surface tension is the dominant effect when the radius is small. Both the viscous force and gravity increase with the radius. However, gravity increases more rapidly than the surface tension with big radius.

References

[1] Tu ZK, Zhang HN, Luo ZP, *et al.* Evaluation of 5 kW Proton Exchange Membrane Fuel Cell Stack Operated at 95 ℃ under Ambient Pressure[J]. J. Power Sources, 2013, 222: 277-281

[2] Pan JJ, Zhang HN, Chen W, *et al.* Nafion-zirconia Nanocomposite Membranes Formed Via in situ Sol-gel Process[J]. *Int. J.Hydrogen Energ.*, 2010, 35: 2 796-2 801

[3] Li K, Ye GB, Zhang HN, *et al.* Self-assembled Nafion/metal Oxide Nanoparticles Hybrid Proton Exchange Membranes[J]. *J. Membrane Sci.*, 2010, 347: 26-31

[4] Yi PY, Peng LF, Feng LZ, *et al.* Performance of A Proton Exchange Membrane Fuel Cell Stack Using Conductive Amorphous Carbon-coated 304 Stainless Steel Bipolar Plates[J]. *J. Power Sources*, 2010, 195 (20), 7 061-7 066

[5] Yi PY, Peng LF, Lai XM, *et al.* A Numerical Model for Predicting Gas Diffusion Layer Failure in Proton Exchange Membrane Fuel Cells [J]. *J. Fuel Cell Sci. Tech.*, 2011, 8 (1): 0110111-01101110

[6] Tang HL, Shen PK, Jiang SP, *et al*. A Degradation Study of Nation Proton Exchange Membrane of PEM Fuel Cells[J]. *J. Power Sources*, 2007, 170: 85-92

[7] Dutta S, Shimpalee S, Van ZJW. Numerical Prediction of Mass Exchange between Cathode and Anode Channels in A PEM Fuel Cell[J]. *Int. J. Heat Mass Tran.*, 2001, 44(11): 2 029-2 042

[8] Pasaogullari U, Wang CY. Two-phase Transport and the Role of Micro-Porous Layer in Polymer Electrolyte Fuel Cells[J]. *Electrochim. Acta*, 2004, 49(25): 4 359–4 369

[9] Nam JH, Kaviany M. Effective Diffusivity and Water-saturation Distribution in Single and Two-layer PEMFC Diffusion Medium [J]. *Int. J. Heat Mass Tran.*, 2003, 46:4 595-4 611

[10] Zhan ZG, Xiao JS, Li DY, *et al.* Effects of Porosity Distribution Variation on Liquid Water Flux through Gas Diffusion Layers of PEM Fuel Cells [J]. *J. Power Sources*, 2006, 160 (2):1 041-1 047

[11] Tuber K, Pocza D, Hebling C. Visualization of Water Buildup in the Cathode of a Transparent PEM Fuel Cell[J]. *J. Power Sources*, 2003, 124: 403-414

[12] Yang XG, Zhang FY, Lubawy AL, *et al.* Visualization of Liquid Water Transport in a PEFC[J]. *Electrochem. Solid St.*, 2004, 7(11): 408-411

[13] Meng H, Wang CY. Electron Transport in PEFCs[J]. *J. Electrochem. Soc.*, 2004, 51(3): A358-A367

[14] Cao ZJ. Dynamic Description of the Phenomena of Dropwise Condensation and the Optimal Contact Angle[J]. *Acta Phys. Sin-Ch. Ed.*, 2002, 51(1): 25-30

[15] Ous T, Arcoumanis C. Visualization of Water Droplets During the Operation of PEM Fuel Cells[J]. *J. Power Sources*, 2007, 173:137–148

[16] Liu X, Guo H, Ma CF. Water flooding and Two-phase Flow in Cathode Channels of Proton Exchange Membrane Fuel Cells[J]. *J. Power Sources*, 2006, 156:267-280

[17] Prat OM, Quintard M, Chane EK, *et al*. Two-phase Flow and Evaporation in Model Fibrous Media: Application to the Gas Diffusion Layer of PEM Fuel Cells [J]. *J. Power Sources*, 2008, 178 :258-268

[18] Djilali N. Computational Modelling of Polymer Electrolyte Membrane (PEM) Fuel Cells: Challenges and Opportunities [J]. *Energy*, 2007, 32: 269-280

[19] Springer TE, Zawodzinski TA, Gottesfeld S. Polymer Electrolyte Fuel Cell Model[J]. *J. Electrochem Soc.*, 1991, 138: 2 334-2 342

[20] Furmidge CL. Studies at Phase Interfaces. Ⅰ. The Sliding of Liquid Drops on Solid Surfaces and A Theory for Spray Retention[J]. *J. Colloid. Sci.*, 1962, 17(4): 309-324

[21] David Q, Azzopardi MJ, Laurent D. Drops at Rest on a Tilted Plane [J]. *Langmuir*, 1998, 14: 2 213-2 216

[22] Yu Y, Tu ZK, Zhan ZG, *et al.* Gravity Effect on the Performance of PEM Fuel Cell Stack with Different Gas Inlet/Outlet Positions[J]. *Int. J. Energ. Res.*, 2012, 36(7):845-855

[23] Hayes R M, Winteron RS. Bubble Diameter on Detachment in Flowing Liquids[J]. *Int. J. Heat Mass Tran.*, 1981,24: 223-230